On the mechanism of protein-templated gold nanoparticle synthesis: Protein organization, controlled gold sequestration, and unexpected reaction products.

*Cassidy Hart, Nouf Abuladel, Madeleine Bee, Megan Channell, Alexander C. CVitan, Moira M. Esson, Andrew Farag, Trisha Ibeh, Eleni N. Kalivas, Daniel-Mario Larco, Andrew Long, Loukas Lymperopoulos, Zachary Mendel, Nancy Miles, Carly Montanero, James C. Schwabacher, Helen Slucher, Javier Vinals, John M. Heddleston[a,†], Douglas M. Fox, Matthew R. Hartings**

Department of Chemistry, American University, 4400 Massachusetts Ave, NW, Washington, DC 20016, USA

[a]Semiconductor and Dimensional Metrology Division, National Institute of Standards and Technology, Gaithersburg, MD 20899, USA

*Corresponding Author – hartings@american.edu

Abstract

Emerging applications that exploit the properties of nanoparticles for biotechnology require that the nanoparticles be biocompatible or support biological recognition. These types of particles can be produced through syntheses that involve biologically relevant molecules (proteins or natural extracts, for example). Many of the protocols that rely on these molecules are performed without a clear understanding of the mechanism by which the materials are produced. We describe a single-pot reaction in which protein-templated gold nanoparticles (AuNPs) are produced as either solution-suspended colloids or as colloids formed within a solid, fibrous protein structure. We have investigated the mechanism for this process by detailing the reaction kinetics and outcomes through the use of 7 different proteins over a range of concentrations and temperatures. The key factor that controls the synthetic outcome (colloid or fiber) is the concentration of the protein relative to the gold concentration. We find that the observed fibrous structures are more likely to form at low protein concentrations and when hydrophilic proteins are used. An analysis of the reaction kinetics shows that AuNP formation occurs faster at lower protein (fiber-forming) concentrations than at higher protein (colloid-forming) concentrations. These results contradict expectations for reaction kinetics and protein-fiber formation, highlighting the need for a better understanding of the mechanism by which biomolecules can facilitate nanoparticle synthesis. As the protein properties that influence this mechanism are better recognized, researchers will be able to better utilize proteins to generate geometry-controlled AuNPs.

Keywords

Biomineralization, Biotemplating, Gold Nanoparticles, Protein Organization, Nanoparticle Bioconjugation, Hierarchical Assembly

1. Introduction

There are a number of strategies for the synthesis of metal nanoparticles (NPs) that rely on naturally sourced or biologically compatible molecules.[1-10] These molecules play an active role in templating NP formation, reducing metal ions, and capping the formed NP. In comparison to syntheses that involve harsh reagents and conditions, protocols using biological molecules are carried out in water and are often considered to be "green." Certainly, though, the primary attraction to using these types of molecules comes from the fact that they can render the NPs biocompatible or can add elements of biological recognition.

As the applications for NPs become more precise, so too do the requirements for controlling NP geometry.[11-15] In this regard, harsh syntheses typically outperform green syntheses. This is not to say that proteins are incapable of facilitating nanostructures with intricate geometries; Nature is filled with instances where biomineralization in complex systems leads to ordered nanometer scale structures.[1, 4] If laboratory syntheses that employ biological molecules are to become technologically relevant, they must be carried out in ways that they precisely control for size and shape. The advancement of green NP syntheses towards this objective is less likely to occur unless their synthetic mechanisms are fully understood.

The green NP synthesis with perhaps the best-understood mechanism is the formation of gold nanoparticles using the Turkevich method.[16] In this reaction, chloroauric acid and citrate ions are boiled in water until the solution becomes maroon in color. Research has shown that AuNP synthesis occurs through several steps: (1) reduction of gold and nucleation of small particles; (2) fast aggregation of the small particles to create intermediate-sized particles; (3) slow aggregation of the intermediate-sized particles; and (4) fast growth these larger particles through incorporation of gold atoms and small particles remaining in solution.[17]

Outside of small molecule studies, researchers have also turned to peptides to better understand how proteins facilitate NP synthesis.[18-20] Several studies have focused on the strict amino acid sequence requirements (reducing amino acids, ligating amino acids, and proximity between these within the peptide chain) that are needed to support NP formation.[18, 19] Additionally, bacterial phages, which display peptides on their surface, have been used to determine sequences that best bind to nanoparticles with specific geometries.[20] Synthetic peptides, mimicking those from the phage experiments, were shown to template the formation of nanoparticles with the same geometries to which they had shown strong binding interactions.

Studies of full proteins and natural extracts, in comparison to the peptide and small molecule systems, are certainly more complex. As there are multiple competing functional groups and reaction pathways, data analysis for discerning the most important influences is not always straightforward. This complexity is not an impediment for producing defined NP structures. The nanoparticles and nanometer-sized features of

natural biominerals (diatom frustules and mollusk shells, among others) are exemplars of the intricacy that can be fashioned in complex systems.[4]

If we are to use proteins in the way that Nature does in biomineralization, we must achieve a better understanding for the way in which different protein properties (size, pI, hydrophobicity, etc) influence the mechanism and output of biotemplating reactions.

In this work, we assess the reaction outcomes and kinetics of a protocol for the formation of gold nanoparticles (AuNPs) in which a protein and tetrachloroaurate ions are incubated in water at elevated temperatures. By testing the protocol with multiple proteins and different reaction conditions, our observations lead to conclusions about which protein properties affect the kinetics of AuNP synthesis.

By controlling the starting conditions, we are also able to dictate the type of reaction product formed. Specifically, protein identity and concentration are coupled to the following outcomes: a homogeneous suspension of AuNPs in solution, AuNPs associated among fibers of proteins (AuNP fibers), extended gold particles, and random precipitates of gold and protein. As the controlled fabrication of two- and three-dimensional arrays of metal nanoparticles has been the topic of some experimental efforts,[21, 22] we have placed a special emphasis in our analysis on studying reactions that result in the formation of the AuNP fibers.

2. Materials and Methods

2.1 Materials

$HAuCl_4 \bullet 3H_2O$, bovine blood hemoglobin (Hb), yeast invertase (Inv), hen egg white lysozyme (Lys), and bovine skeletal myoglobin (Mb) were purchased from Sigma. Bovine serum albumin (BSA) was purchased from Calbiochem. Beef liver catalase (Cat) was purchased from Spectrum. Porcine Pepsin 1:3000 (Pep) was purchased from Amresco. The Au standard for atomic absorption was purchased from Inorganic Ventures. De-ionized water (> 16 MΩ) was obtained from a Barsted E-pure 3-module water purification system.

2.2 Synthetic Protocol and Sample Preparation

AuNP-protein material synthesis occurs as follows. An aqueous solution containing 250 μM $HAuCl_4$ and protein (with a concentration between 0.64 μM and 25 μM) is heated in a covered container. For the analysis of reaction products, 5 mL of this solution is added to a test tube, which is covered in aluminum foil, and heated for 4 hours at 80 °C. To analyze reaction kinetics, 3 mL of solution is added to a quartz cuvette, which is covered with a Teflon cap, and heated as described below.

2.3 Reaction product: Solution analysis

The aqueous portion of the reaction product was analyzed with UV-Vis and atomic absorption (AA) spectroscopies. Prior to measurement, all samples were centrifuged (Sorvall RC 6+ with an SH-3000 rotor) at 4000 rpm for 30 minutes to remove any non-suspended material. UV-Vis spectra were recorded using a Shimadzu UV-2550 instrument. AA spectra were recorded using a Shimadzu AA-6200 instrument. UV-Vis spectra can indicate the presence of protein (absorbance maximum ~ 280 nm), Au^{3+} (absorbance maximum ~ 325 nm), and AuNP-protein (absorbance maximum ~ 530 nm)

in solution. AA spectra indicate the presence of Au, as Au^{3+}, Au^{+} or Au^{0}, in solution but is unable to distinguish between these.

2.4 Reaction product: Analysis of solids formed

Transmission electron microscopy (TEM) images were recorded using a Philips Electronic Instruments Company EM400T instrument and analyzed using the AnalySIS FIVE software program. Suspensions of AuNP-protein fiber solutions were placed on copper TEM grids and allowed to evaporate. Scanning electron microscopy (SEM) samples were prepared by adding suspensions of protein-AuNP fibers to conductive tape and allowing the water to evaporate. The samples were sputter coated with a Hummer Sputtering System utilizing "Ultra Carbon 'F' Purity" (Ultra Carbon Corp., Bay City, MI) electrodes. Scanning Electron Microscopy (SEM) images were collected using a Joel JSM-6360LV system in secondary electron imaging mode.

2.5 Analysis of reaction kinetics: video

A fiber formation reaction was recorded for lysozyme at an Au:protein ratio of 45. A capped scintillation vial with 20 mL of reaction solution was placed in a water bath at 80 °C and recorded with a video camera. The full video is included in the supplementary file.

2.6 Analysis of reaction kinetics: UV-Vis spectroscopy

Reaction kinetics were observed using UV-Vis spectroscopy as measured with an Ocean Optics Jaz spectrometer with an Ocean Optics DH-2000 light source. Teflon-capped cuvettes containing reaction samples were placed within a qpod 2e cuvette holder from

Quantum Northwest. Reactions were monitored at 60, 70, 80, and 90 °C and were allowed to proceed for an appropriate amount of time such that nanoparticle formation (as defined by the absorption of the localized surface plasmon resonance, LSPR, feature) had neared completion (anywhere between 2 and 18 hours). Nanoparticle formation kinetics were analyzed by subtracting the absorption minimum (located between 430 nm and 480 nm) from the LSPR maximum (located between 530 nm and 590 nm). This subtraction was performed to account for variations in excitation light intensity over the course of the experiment.

3. Results

3.1 Analysis of reaction products

Each studied protein (BSA, catalase, hemoglobin, invertase, lysozyme, myoglobin, and pepsin) can facilitate an observable reaction with the gold. Syntheses using BSA, catalase, hemoglobin, lysozyme, or myoglobin all result in two outcomes: purple solutions at high protein concentrations and purple fibers suspended in solution at low protein concentrations. Figure 1 shows a picture of the fibrous material. The homogeneous suspensions of colloidal AuNPs are similar to what other studies of protein-templated AuNPs have described.[23-25] Photographs of all reaction products can be found in the Supporting Information. At concentrations of 50 μM and higher there is no observable difference between the solution at the start and end of the reaction. Samples with invertase all resulted in the formation of precipitates at the bottom of the test tubes (Supporting Information). At the highest invertase concentration, the precipitate is yellowish while the lower invertase concentrations result in purple precipitates. Samples

with pepsin resulted in either dark precipitate at the bottom of the test tube (high concentrations) or a suspension of dark purple particulate material (low concentrations).

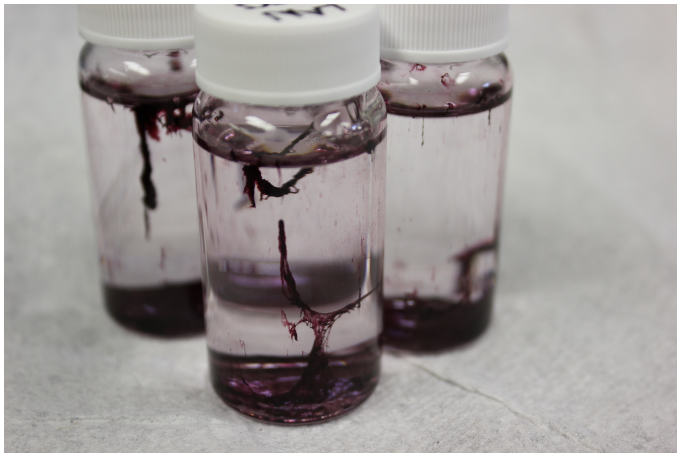

Figure 1. Photograph of the AuNP containing fibers formed during the reaction between lysozyme (5.56 μM) and $HAuCl_4$ (250 μM).

TEM and SEM analysis provide a more detailed view of these reaction products. The purple solutions are comprised of a homogeneous suspension of nanoparticles similar to the nanoparticles that are made using similar procedures.[23-25] For that reason, EM images of these samples are not presented here. The SEM images of the samples with suspended purple fibers are generally similar, regardless of the protein used to prepare them. Figure 2 shows a representative SEM image and TEM image of a fiber sample.

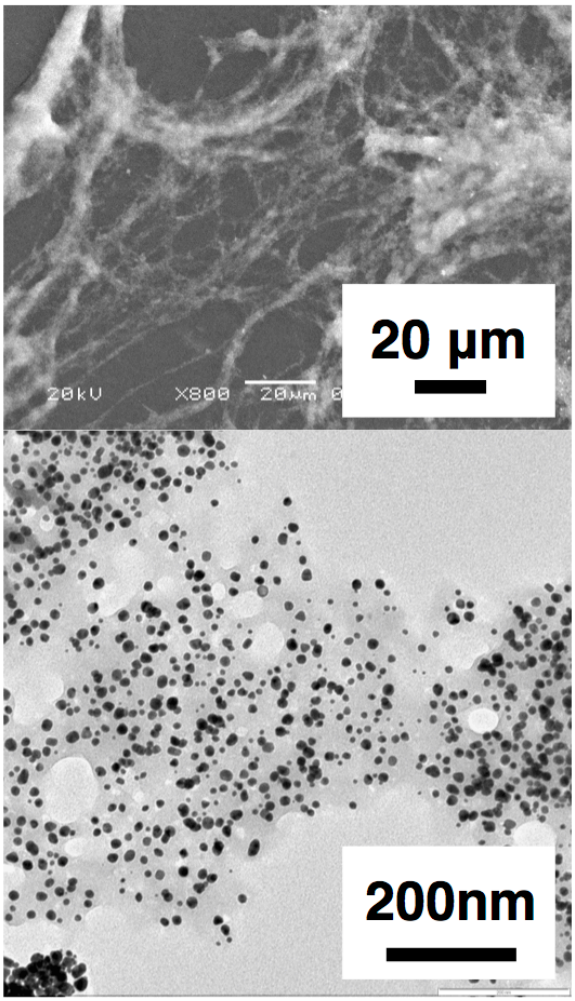

Figure 2. SEM image (top panel) and TEM image (bottom panel, 5.56 µM lysozyme) images of AuNPs incorporated into protein fibers.

The SEM image shows that most of the fibers are < 5 µm in diameter. Upon closer inspection, this material appears to be more of a network of well-defined strands and points of intersection. The nanoparticles are clearly visible in the TEM image (dark spots). Also visible is the protein fiber, which stands out as a very light gray against the background. All fiber-forming proteins (BSA, catalase, hemoglobin, lysozyme, and myoglobin) show similar features in their TEM images (Supporting Information). One difference between fiber-forming samples is the sizes of the AuNPs. The biotemplating reaction with some proteins results in smaller AuNPs. BSA and lysozyme produce

AuNPs that are mostly 20 nm and smaller. Catalase, myoglobin and hemoglobin produce larger AuNPs (as small as 20 nm and as big as 100 nm). Hemoglobin and myoglobin, in particular, qualitatively show less homogeneity in AuNP sizes than do the other fiber forming proteins (Figure 3).

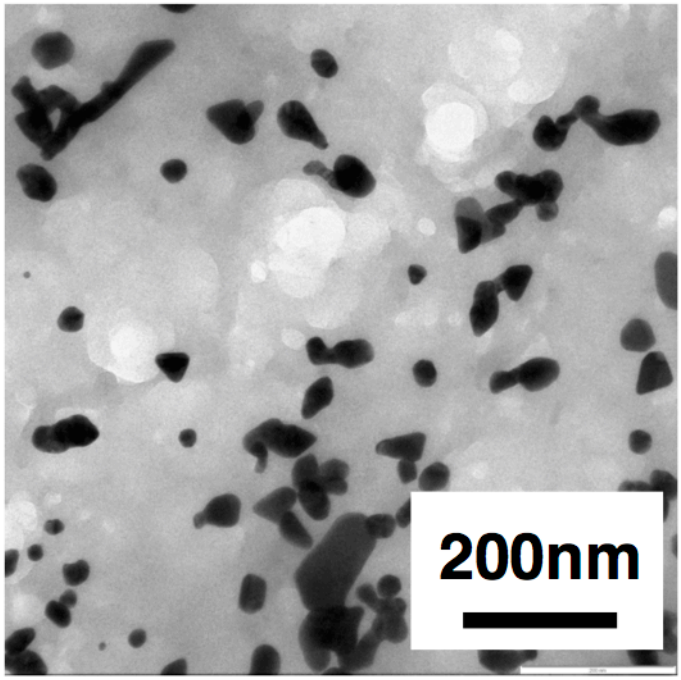

Figure 3. TEM image of AuNPs formed using 5.2 μM hemoglobin.

The TEM image of invertase samples (Supporting Information) is similar to those for the fiber-forming proteins. AuNPs, generally 20 nm in diameter and smaller, are seen among a light gray material.

TEM images of pepsin samples, which were the only samples that produced dark precipitates, display a unique reaction product when compared to the other samples we prepared. Figure 4 shows that the AuNP-pepsin composite materials consist of extended and amorphous gold particles with some observed light gray material that we assume is mostly protein in nature.

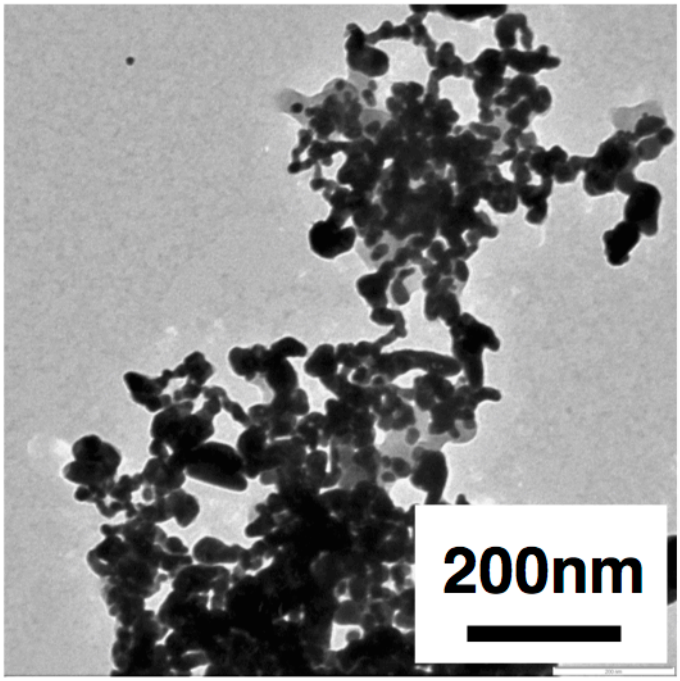

Figure 4. TEM image of the pepsin biotemplating reaction at a Au:Pep ratio of 70 (scale bar is 200 nm).

UV-Vis spectroscopy and atomic absorption (AA) spectroscopy were used to evaluate the reaction products. UV-Vis can assist in distinguishing between unreacted $HAuCl_4$ (absorbance feature near 320 nm) and the presence of AuNPs (absorbance feature at longer wavelengths 520 nm – 700 nm). Most AuNPs in our study had absorption features closer to the 530 nm – 550 nm range. The location of these absorption features generally corresponds to their size; larger AuNPs have absorption features that appear at longer wavelengths.[26] AA spectroscopy was used to note the concentration of total gold (at any oxidation state) in solution. This measurement tracks the gold that remains in solution for the fiber forming samples.

Figure 5 shows an analysis of the UV-Vis and AA data for catalase. The Au solution concentration is noted by the closed circles. The open squares denote the absorption intensity of the LSPR feature. These values have been normalized to the highest value

observed for this feature across all catalase concentrations. That is, a maximum yield of nanoparticles is observed at 3.3 μM (or an Au:catalase ratio of 75).

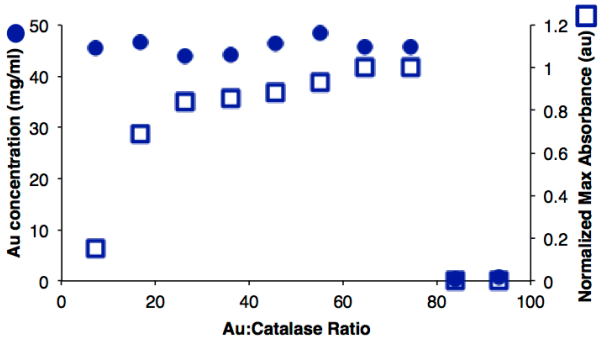

Figure 5. Analyzed UV-Vis and AA data for the biotemplating reaction with catalase at multiple protein concentrations. The closed circles correspond to the Au concentration measured by AA (in mg/mL). The open squares correspond to the normalized LSPR absorption intensity.

There are several relevant segments in this graph. At high protein concentrations (low Au:protein ratios) very little AuNPs are formed. Only when the protein concentration is decreased is there any observable production of AuNPs. The yield of AuNP increases with decreasing protein concentration until the concentration becomes too low (< 3.1 μM) and no AuNPs are observed in solution. This drop-off corresponds to the transition from the generation of homogeneous suspensions of AuNPs to AuNPs associated with protein fibers. The AA data also show a change at this point, from a near constant concentration for low ratios to no observable gold in solution at high ratios. While no measureable Au remains in solution, the photographs of the reaction products and the TEM data indicate that AuNPs are found in the fibrous materials. The UV-Vis and AA data show that when fibers are formed AuNPs and any unreacted $AuCl_4^-$ are sequestered within the solid material. These generic observations (no NP formation at high protein

concentrations, homogeneous suspensions of AuNPs formed at intermediate concentrations, and formation of AuNPs within fibers at low protein concentrations) hold for all of the proteins that form fibers (BSA, catalase, hemoglobin, lysozyme, and myoglobin). Full UV-Vis data sets and the analyzed UV-Vis/AA data for all proteins can be found in the Supporting Information.

3.2 Analysis of AuNP formation kinetics

The difference between AuNP formation in reactions that resulted in homogeneously suspended AuNPs and those that resulted in AuNPs interspersed among protein-based fibers was surprising to us. We did not expect such a sharp transition in reaction products with changing protein concentration. To probe these regimes more closely, we explored the kinetics of AuNP formation during fiber synthesis and during homogeneous AuNP synthesis.

The images in Figure 6 are still frame images from a video we recorded of the AuNP fiber forming reaction. There are three notable time domains from this video. Fibers start appearing in the earliest of these domains and are characterized by their yellowish hue. As time goes on, the yellow turns into a lighter purple and then darker shade of purple. Absent from these images is the presence of any notable purple coloration in the solution surrounding the fibers. This observation is consistent with the UV-Vis and AA data that all of the gold is incorporated amongst the fibrous composite material. Purple coloration within the fibers, and its absence in solution, indicates that AuNP formation only occurs within this solid material. That is, AuNPs do not form in solution and then diffuse into

the fibers, and protein-ligated AuNPs do not first form as part of a homogeneous suspension in water and then subsequently organize into fibers.

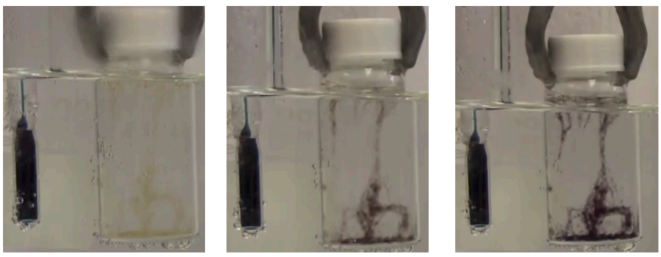

Figure 6. Images from a video recording of a fiber formation reaction (0.25 mM $HAuCl_4$ and 5.6 μM lysozyme in 20 mL of water heated at 80 °C).

We measured the kinetics of AuNP formation for each of the fiber forming proteins (BSA, catalase, hemoglobin, lysozyme, and myoglobin) at concentrations where the reaction would result in either suspended AuNPs or AuNPs incorporated among fibers. We performed observed these reactions using UV-Vis spectroscopy while maintaining temperatures of 60, 70, 80, or 90 °C.

As the light source fluctuated over the course of these measurements, sometimes spanning over 18 hours, we had to analyze the data in a manner in which these fluctuations would not influence the observations. We noted the LSPR wavelength of maximum absorbance and the absorbance minimum that occurs at slightly higher wavelengths than the LSPR (Supporting Information) of the final spectrum taken during an experiment. We calculated the change in absorption at every time point for these wavelengths, $\Delta A = A(\lambda_{LSPRmax}) - A(\lambda_{min})$. Assessing the kinetics of AuNP formation within the fibers added a different layer of complexity to the analysis. Because the AuNPs are not spread throughout solution and are confined to very specific locations, the

absolute absorbance measurement is meaningless within this context. What can be observed by the absorbance measurements for AuNP formation within the protein fibers are the changes of absorbance as the reaction progresses to the endpoint, at which no further change is measured. That is, when the absorbance reaches a steady state, the reaction is near completion. What was important for this study was to understand how nanoparticle production progressed toward its endpoint. For some of our measurements, there was very little fiber located in the path the light traveled through the cuvette. In other measurements, there was more signal as more of the fibrous material was in a better location. For each case, the steady state absorbance signaled the reaction was nearing its endpoint. For this reason, we normalized ΔA to ΔA_{min} and ΔA_{max}.

Figure 7 shows the AuNP formation kinetics for myoglobin at Au:myoglobin ratios of 45 (homogeneous suspension of AuNPs) and 55 (AuNPs associated with protein fibers). These measurements were taken at 60, 70, 80 and 90 °C. As expected, the AuNP formation reaction proceeds faster as the temperature increases. At every temperature, AuNP production is faster for the cases where fibers are formed than for the cases where homogeneous suspensions of AuNPs are formed. For the experiments shown in Figure 6, the myoglobin concentrations were 5.6 μM (Au:protein = 45) and 4.5 μM (Au:protein = 55).

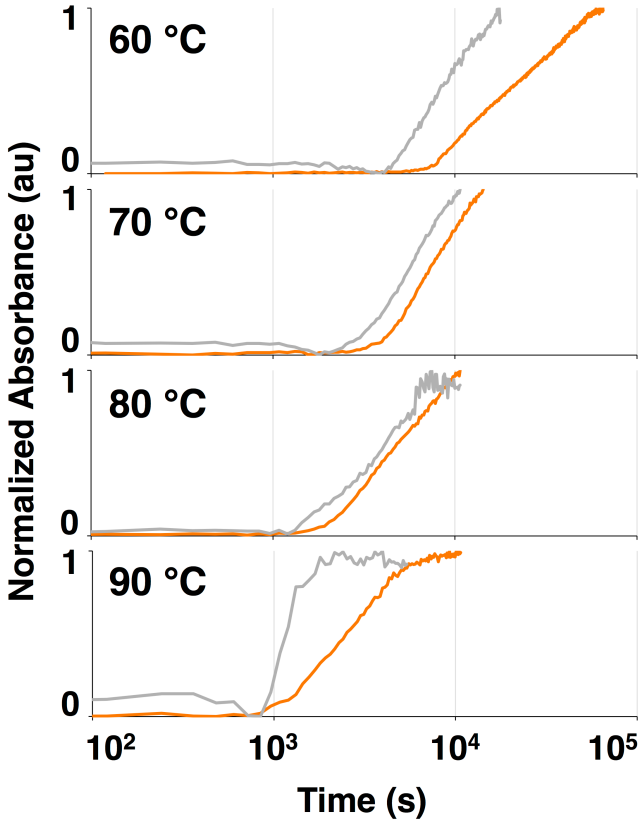

Figure 7. Synthesis of AuNPs at multiple temperatures and in reaction conditions which produce either homogeneous myoglobin-AuNPs (orange line, Au:myoglobin ratio = 45) or myoglobin-AuNP fibers (gray line, Au:myoglobin ratio = 55).

These observations hold for the other fiber-forming proteins from this study as well (see Supporting Information). AuNP formation occurs faster for the cases where fibers are formed than the cases where AuNPs are formed as part of a homogeneous suspension. That is, the rate of AuNP production is faster at lower protein concentrations than at higher protein concentrations.

We tested this conclusion by studying the AuNP formation reaction at 80 °C for individual proteins across multiple concentrations. Figure 8 shows these experiments for BSA and hemoglobin. For each protein, 3 sets of reactions result in homogeneous suspensions of nanoparticles and 1 set that results in fibers with incorporated AuNPs. The

absorbance values are not normalized for this graph. As the concentration goes down (Au:protein ratio goes up), the rate of nanoparticle formation becomes faster. This observation is most pronounced for BSA.

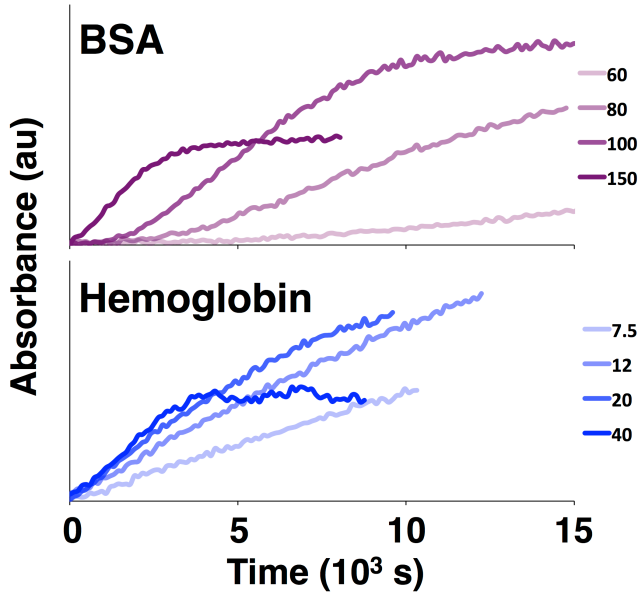

Figure 8. AuNP formation reactions for BSA (top panel) and hemoglobin (bottom panel) at different protein concentrations. The legend shows the different Au:protein ratios. For BSA these ratios were 60, 80, 100, and 150, which correspond to BSA concentrations of 4.2, 3.1, 2.5, and 1.7 μM, respectively. For hemoglobin, the ratios were 7.5, 12, 20, and 40, which correspond to hemoglobin concentrations of 33.3, 20.8, 12.5, and 6.3 μM, respectively. AuNPs are formed among protein fibers for BSA at a ratio of 150 and hemoglobin at a ratio of 40.

4. Discussion

There is a real need to provide biocompatible NPs with defined shape and size for new technological applications.[27-31] There are numerous examples of the use of biological polymers and natural extracts to synthesize these types of NPs.[1-10, 23-25] In general, these experiments tend to focus on which natural materials enable NP synthesis and what applications the resulting NPs might be useful for. Further mechanistic understanding can

lead to syntheses that yield geometry-controlled nanoparticles and would improve our ability to exploit natural biomineralization processes, enabling the discovery and production of novel biomaterials. As a result of the mechanistic studies communicated here, we present both: kinetic details and protein-property controls over templated AuNP synthesis, and a description of an organized, solid material in which AuNPs are associated with fibers of proteins.

The most general protein property that affects the biotemplating reaction studied here is concentration. Our results suggest that protein concentration has some unexpected influences on the biotemplating reaction that we have performed. First, concentration affects the identity of the reaction outcome. AuNPs are formed within fibers of proteins at low protein concentrations and homogeneous suspensions of AuNPs are formed at high protein concentrations. Within the context of protein fiber formation, especially proteins relevant to amyloid diseases, the expectation is that protein fibers are formed at high protein concentrations. In combination with data discussed below, our protocol presents a different context to generate protein fibers: biotemplating nanoparticles.

Concentration also affects the rate of nanoparticle formation in counterintuitive ways; AuNP synthesis occurs faster at lower protein concentrations. Figures 7 and 8 show that this is the case whether the AuNP formation is occurring in protein fibers or in solution. While traditional kinetics theory would make one think that reaction rates should increase with increasing concentrations, there are reports in the literature that show why this might not be the case for our system. Mirsaidov and colleagues have observed AuNP formation dynamics with TEM.[32] Initially, gold is homogeneously spread throughout the solution. The first step in the formation of AuNPs involves spinodal decomposition, in which

islands of gold-rich areas form amid gold-poor regions of solvent. This process is driven by small changes in local density, driving a solution to demix.

In our experiments, it is conceivable that the proteins (specifically their capacity to organize gold ions through coordination) assist in driving the production of gold rich regions. As the protein concentration decreases, there are fewer sites to nucleate these localized gold phases. Although fewer individual sites exist, these sites are still able to drive spinodal decomposition. In experiments with high concentrations of proteins, there are many sites driving the formation of gold phases. The gold is spread across all of these sites. In experiments with low concentrations of proteins, the lower number of sites still segregates the same amount of gold. Thus, for the low protein concentration environment, the local concentration of gold is higher where gold nanoparticle formation is occurring.

Similar to the gold systems we present here, researchers studying the formation of calcium-based minerals in more biologically relevant systems have found that proteins are capable of inducing what is often termed a "polymer-induced liquid precursor" (PILP) phase.[10, 33-35] This PILP phase, in which the mineral phase organizes in an amorphous and fluid nature, constitutes a necessary step in the formation of mineral particles from aqueous solution. Gower and colleagues have specifically shown that, in a low protein concentration environment, the activation energy for formation of this PILP phase is lower than the activation energy for the corresponding systems at higher protein concentrations.[33]

These precedents demonstrate the importance of generating gold-rich amorphous phases and help to explain the formation of the fibers that we have described here. Proteins can facilitate the production of gold-rich regions within a reaction solution. As the protein concentration decreases, spinodal decomposition can bring multiple gold phases together, and with these, the proteins with which they are associated. In effect, we are observing the formation of the protein-based fibers driven by the kinetics of nanoparticle formation.

Biomineralization or biotemplating, then, offers a new context with which to generate and synthesize protein-based materials. Typically, this has involved exploiting high concentrations of hydrophobic proteins to form one-dimensional fibers. Tezcan and colleagues have shown how metal coordination can lead to the production of organized materials.[36] The development of new protein-based materials, however, has traditionally been left to using simple hydrophobic-hydrophilic interactions to drive their formation.[37-39] This has left a gap in our ability to mimic Nature, which uses proteins to drive the formation of nano-scale and macro-scale material architecture. While researchers have become proficient at designing materials with intricate geometry using DNA origami,[40-43] the ability to design and generate materials with proteins remains elusive. Additionally, there is a push to develop materials in which nanoparticles are organized and arranged over long length scales in multiple dimensions. Again, DNA has primarily been used to template some materials that push towards this goal.[21, 22, 41] We have herein demonstrated that the kinetics of biotemplating has the potential to organize nanoparticles into protein-based materials.

For these reasons, we investigated the production of the AuNP-protein fiber material more closely. (The protein properties data we used for this analysis can be found the

Supporting Information.) The Au:protein ratio that characterizes the boundary between the formation of homogeneous suspensions of AuNPs and the production of AuNPs within protein fibers varies with the identity of protein used. Several properties, examined for their ability to determine this critical Au:protein ratio, could be immediately eliminated. Protein molecular weight, percent of protein that is structured, protein isoelectric point, and protein unfolding temperatures showed no correlation to this ratio. Two properties that have been noted in their ability to control metal nanoparticle formation by peptides, number of ligating amino acids and number of reducing amino acids, do show a linear correlation to the critical ratio (Figure 9). As these are the amino acids responsible for coordinating with the gold and converting the gold from Au(III) to Au(0), it is not surprising that they would play some role in the formation of these AuNP fibers as well.

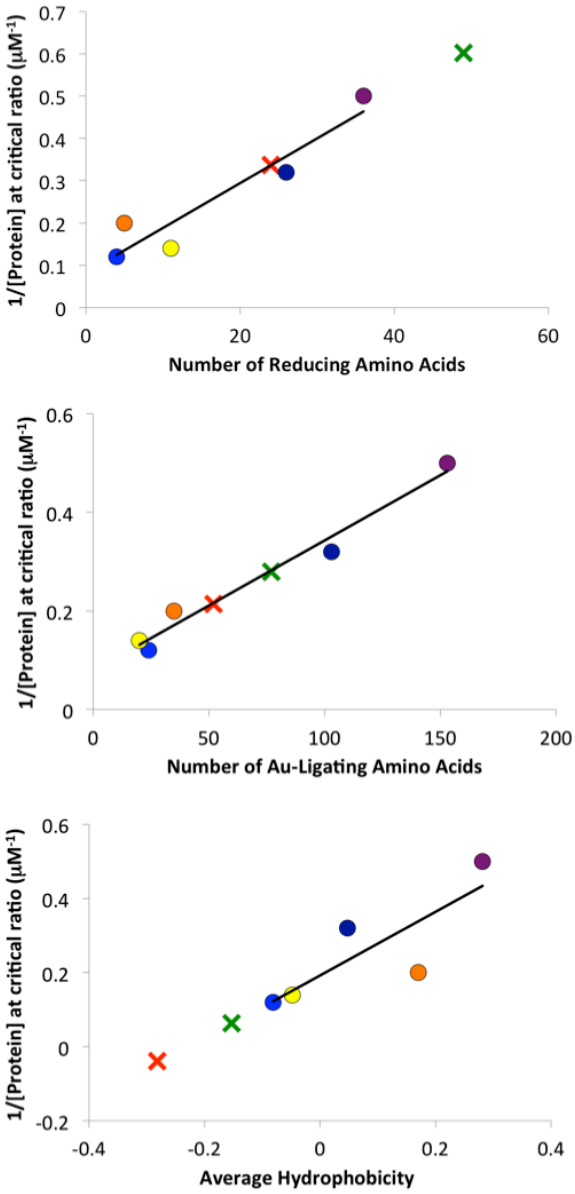

Figure 9. Correlation between critical Au:protein ratio ($[protein]^{-1}$) and several protein properties. The top panel shows the correlation to the number of reducing amino acids, the middle panel to the number of gold-ligating amino acids, and the bottom panel to the average protein hydrophobicity. The circles (purple: BSA; dark blue: catalase; light blue: hemoglobin; yellow: lysozyme; and orange: myoglobin) correspond to proteins that facilitate the production of AuNP fibers. The × symbols correspond to proteins that do not form AuNP fibers (green: invertase; red: pepsin) are extrapolated to the graphs based upon the values that describe their numbers of reducing amino acids, numbers of ligating amino acids, and average hydrophobicity.

However, the numbers of ligating and reducing amino acids alone are not able to explain why some proteins do not form the AuNP-protein fibers. For these protein properties, the correlations predict that invertase and pepsin should not be excluded from forming AuNP fibers. When correlated to average protein hydrophobicity, the correlation predicts that both invertase and pepsin fall outside of the range of hydrophobicity values of the fiber forming proteins, matching our observations. This evaluation suggests that both invertase and pepsin are too hydrophobic to allow for the formation of AuNP fibers. In this description, the interaction between proteins (driven by hydrophobic interactions) would dominate the kinetics in a way that would prevent biotemplating-driven fiber formation.

Conclusions

We have analyzed the mechanism and results of a protein-templated synthesis of gold nanoparticles. Protein identity and concentration determine which reaction products are formed, most notably novel protein fibers that incorporate AuNPs. Our data indicate the amorphous, gold-rich phases, supported by the presence of proteins, are a likely step in the reaction pathway. With a better understanding of its kinetic mechanism, this reaction can be harnessed in new ways to support the synthesis of geometry-defined gold nanoparticles. The protocol has also produced a unique material, AuNP-protein fibers, which provide a novel platform for exploring artificial biomineralization and designing materials that systematically array both gold nanoparticles and proteins over multiple length scales.

References

1. M. B. Dickerson, K. H. Sandhage and R. R. Naik, *Chem. Rev.*, 2008, **108**, 4935-4978.
2. S. Weiner and L. Addadi, *J. Mat. Chem.*, 1997, **7**, 689-702.
3. M. R. Hartings, N. Benjamin, F. Briere, M. Briscione, O. Choudary, T. L. Fisher, L. Flynn, E. Ghias, M. Harper, N. Khamis, C. Koenigsknecht, K. Lazor, S. Moss, E. Robbins, S. Schultz, S. Yaman, L. M. Haverhals, P. C. Trulove, H. C. De Long, A. E. Miller and D. M. Fox, *Sci. Technol. Adv. Mat.*, 2013, **14**.
4. W. J. Crookes-Goodson, J. M. Slocik and R. R. Naik, *Chemical Society Reviews*, 2008, **37**, 2403-2412.
5. H. H. Duan, D. S. Wang and Y. D. Li, *Chemical Society Reviews*, 2015, **44**, 5778-5792.
6. S. Iravani, *Green Chemistry*, 2011, **13**, 2638-2650.
7. A. K. Mittal, Y. Chisti and U. C. Banerjee, *Biotechnology Advances*, 2013, **31**, 346-356.
8. M. M. Unterlass, *European Journal of Inorganic Chemistry*, 2016, 1135-1156.
9. S. F. Adil, M. E. Assal, M. Khan, A. Al-Warthan, M. R. H. Siddiqui and L. M. Liz-Marzan, *Dalton Transactions*, 2015, **44**, 9709-9717.
10. D. C. Bassett, L. M. Grover, F. A. Muller, M. D. McKee and J. E. Barralet, *Advanced Functional Materials*, 2011, **21**, 2968-2977.
11. N. Semagina and L. Kiwi-Minsker, *Catalysis Reviews-Science and Engineering*, 2009, **51**, 147-217.
12. M. X. Yu and J. Zheng, *ACS Nano*, 2015, **9**, 6655-6674.
13. Q. B. Zhang, J. P. Xie, Y. Yu and J. Y. Lee, *Nanoscale*, 2010, **2**, 1962-1975.
14. M. A. El-Sayed, *Acc. Chem. Res.*, 2004, **37**, 326-333.
15. Y. Yin and A. P. Alivisatos, *Nature*, 2005, **437**, 664-670.
16. B. V. Enustun and J. Turkevich, *J. Amer. Chem. Soc.*, 1963, **85**, 3317-3328.
17. J. Polte, T. T. Ahner, F. Delissen, S. Sokolov, F. Emmerling, A. F. Thunemann and R. Kraehnert, *J. Amer. Chem. Soc.*, 2010, **132**, 1296-1301.
18. R. Coppage, J. M. Slocik, B. D. Briggs, A. I. Frenkel, R. R. Naik and M. R. Knecht, *ACS Nano*, 2012, **6**, 1625-1636.
19. Y. N. Tan, J. Y. Lee and D. I. C. Wang, *J. Amer. Chem. Soc.*, 2010, **132**, 5677-5686.
20. C.-Y. Chiu, Y. Li, L. Ruan, X. Ye, C. B. Murray and Y. Huang, *Nat Chem*, 2011, **3**, 393-399.
21. R. J. Macfarlane, M. R. Jones, B. Lee, E. Auyeung and C. A. Mirkin, *Science*, 2013, **341**, 1222.
22. Y. Kim, R. J. Macfarlane, M. R. Jones and C. A. Mirkin, *Science*, 2016, **351**, 579.
23. M. S. Bakshi, H. Kaur, T. S. Banipal, N. Singh and G. Kaur, *Langmuir*, 2010, **26**, 13535-13544.
24. J. L. Burt, C. Gutierrez-Wing, M. Miki-Yoshida and M. Jose-Yacaman, *Langmuir*, 2004, **20**, 11778-11783.
25. F. Canaveras, R. Madueno, J. M. Sevilla, M. Blazquez and T. Pineda, *Journal of Physical Chemistry C*, 2012, **116**, 10430-10437.

26. W. Haiss, N. T. K. Thanh, J. Aveyard and D. G. Fernig, *Analytical Chemistry*, 2007, **79**, 4215-4221.
27. I. Lynch, T. Cedervall, M. Lundqvist, C. Cabaleiro-Lago, S. Linse and K. A. Dawson, *Advances in Colloid and Interface Science*, 2007, **134-35**, 167-174.
28. J. Xie, G. Liu, H. S. Eden, H. Ai and X. Y. Chen, *Acc. Chem. Res.*, 2011, **44**, 883-892.
29. C. Amiens, D. Ciuculescu-Pradines and K. Philippot, *Coordination Chemistry Reviews*, 2016, **308**, 409-432.
30. Z. Q. Chu, S. L. Zhang, B. K. Zhang, C. Y. Zhang, C. Y. Fang, I. Rehor, P. Cigler, H. C. Chang, G. Lin, R. B. Liu and Q. Li, *Scientific Reports*, 2014, **4**.
31. M. Shilo, A. Sharon, K. Baranes, M. Motiei, J. P. M. Lellouche and R. Popovtzer, *Journal of Nanobiotechnology*, 2015, **13**.
32. N. D. Loh, S. Sen, M. Bosman, S. F. Tan, J. Zhong, C. A. Nijhuis, P. Král, P. Matsudaira and U. Mirsaidov, *Nat Chem*, 2016, **advance online publication**.
33. M. A. Bewernitz, D. Gebauer, J. Long, H. Colfen and L. B. Gower, *Faraday Discussions*, 2012, **159**, 291-312.
34. J. S. Evans, *Crystengcomm*, 2013, **15**, 8388-8394.
35. L. B. Gower, *Chem. Rev.*, 2008, **108**, 4551-4627.
36. E. N. Salgado, R. J. Radford and F. A. Tezcan, *Acc. Chem. Res.*, 2010, **43**, 661-672.
37. H. Acar, R. Genc, M. Urel, T. S. Erkal, A. Dana and M. O. Guler, *Langmuir*, 2012, **28**, 16347-16354.
38. A. J. Baldwin, T. P. J. Knowles, G. G. Tartaglia, A. W. Fitzpatrick, G. L. Devlin, S. L. Shammas, C. A. Waudby, M. F. Mossuto, S. Meehan, S. L. Gras, J. Christodoulou, S. J. Anthony-Cahill, P. D. Barker, M. Vendruscolo and C. M. Dobson, *J. Amer. Chem. Soc.*, 2011, **133**, 14160-14163.
39. T. P. J. Knowles, T. W. Oppenheim, A. K. Buell, D. Y. Chirgadze and M. E. Welland, *Nat. Nanotechnol.*, 2010, **5**, 204-207.
40. V. Linko and H. Dietz, *Current Opinion in Biotechnology*, 2013, **24**, 555-561.
41. L. H. Tan, H. Xing and Y. Lu, *Acc. Chem. Res.*, 2014, **47**, 1881-1890.
42. M. R. Jones, N. C. Seeman and C. A. Mirkin, *Science*, 2015, **347**.
43. F. Praetorius and H. Dietz, *Science*, 2017, **355**.

Supplemental information for:
On the mechanism of protein-templated gold nanoparticle synthesis: Protein organization, controlled gold sequestration, and unexpected reaction products.

*Cassidy Hart, Nouf Abuladel, Madeleine Bee, Megan Channell, Alexander C. CVitan, Moira M. Esson, Andrew Farag, Trisha Ibeh, Eleni N. Kalivas, Daniel-Mario Larco, Andrew Long, Loukas Lymperopoulos, Zachary Mendel, Nancy Miles, Carly Montanero, James C. Schwabacher, Helen Slucher, Javier Vinals, John M. Heddleston[a,†], Douglas M. Fox, Matthew R. Hartings**
Department of Chemistry, American University, 4400 Massachusetts Ave, NW, Washington, DC 20016, USA
[a]Semiconductor and Dimensional Metrology Division, National Institute of Standards and Technology, Gaithersburg, MD 20899, USA
*Corresponding Author – hartings@american.edu

Contents

I. Protein-AuNP and protein-AuNP fiber reaction products.

BSA-AuNP reaction products

A full set of reaction products for BSA can be found in one of our previous publications.[1]

S1. Catalase-AuNP reaction products

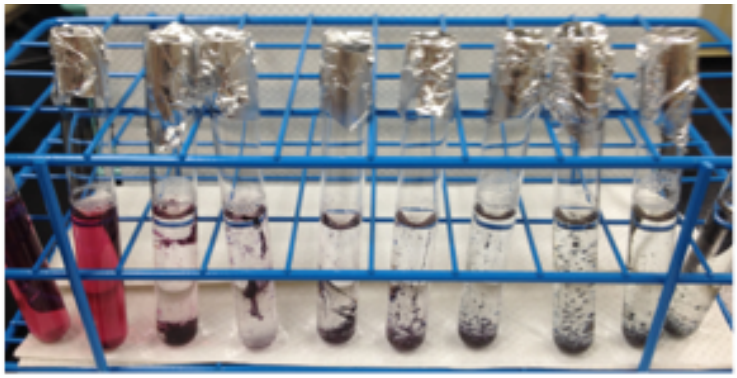

Au:Catalase Ratio 30 70 110 150 190 230 270 310 350 390

S2. Hemoglobin-AuNP reaction products

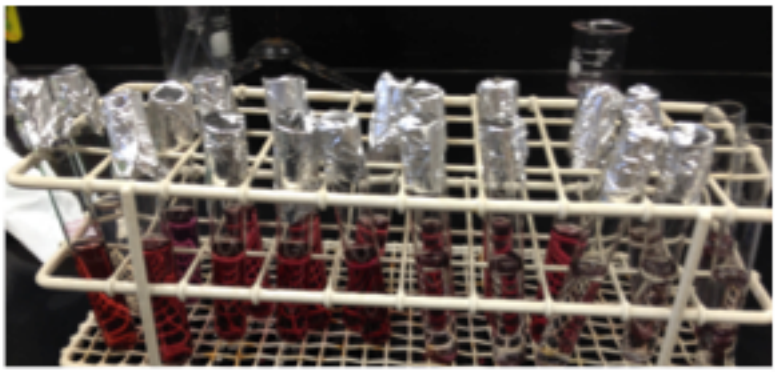

Au:Hb Ratio 7.5 13 18 23 28 33 38 43 48 53

S3. Invertase-AuNP reaction products

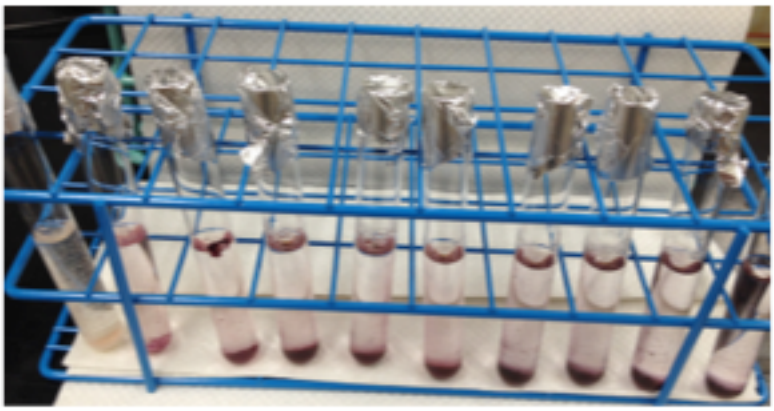

Au:Pepsin Ratio 30 70 110 150 190 230 270 310 350 390

S4. Lysozyme-AuNP reaction products

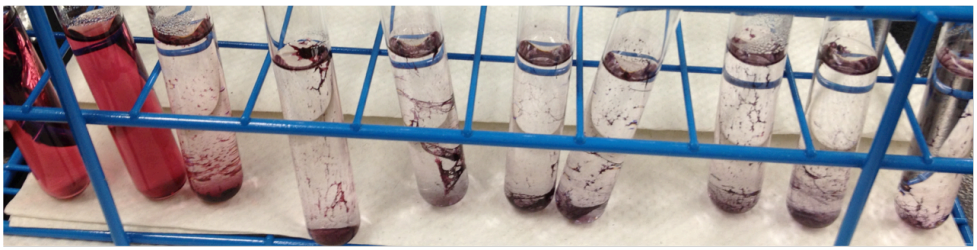

25 30 35 40 45 50 55 60 65 70
Au:Lysozyme ratio

S5. Myoglobin-AuNP reaction products

Au:Mb ratios

20 30 40 50 60 70 80 90 100 ∞

S6. Pepsin-AuNP reaction products

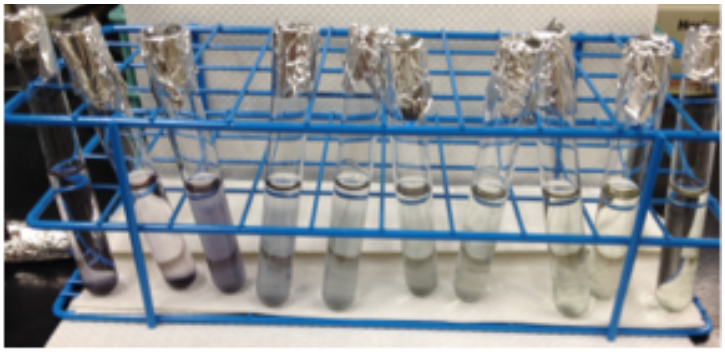

Au:Pepsin Ratio 30 70 110 150 190 230 270 310 350 390

II. TEM data

TEM images were taken using a Philips Electronic Instruments Company EM400T instrument and analyzed using the AnalySIS FIVE software program. In all images, the scale bar is 200nm.

S7. TEM image of BSA-AuNP fibers at a Au:BSA ratio of 125

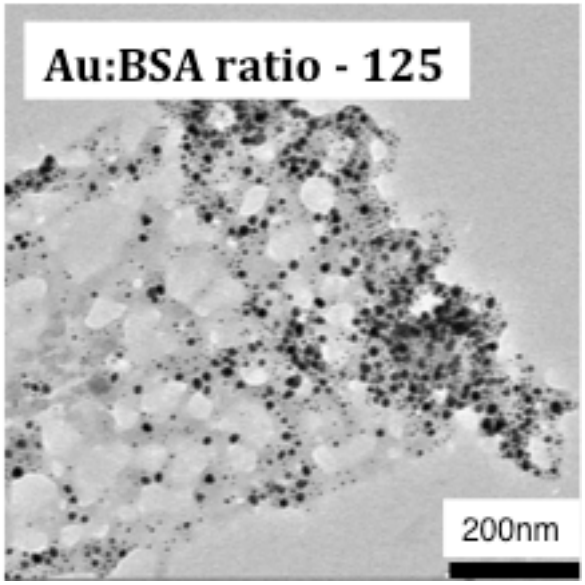

S8. TEM image of Catalase-AuNP fibers at a Au:Catalase ratio of 150

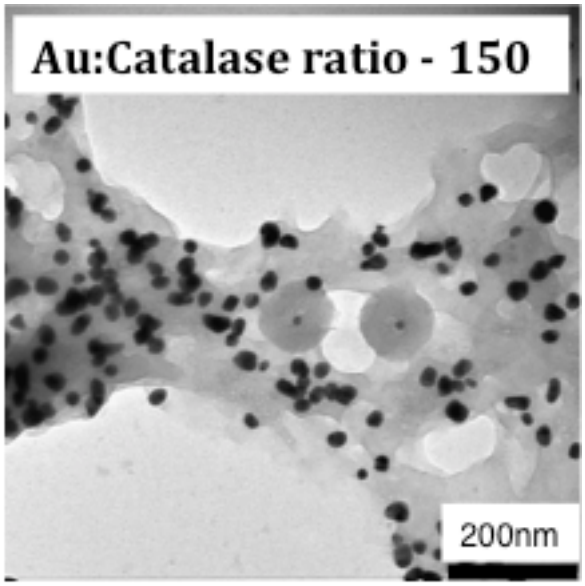

S9. TEM image of Invertase-AuNP fibers at a Au:Invertase ratio of 70

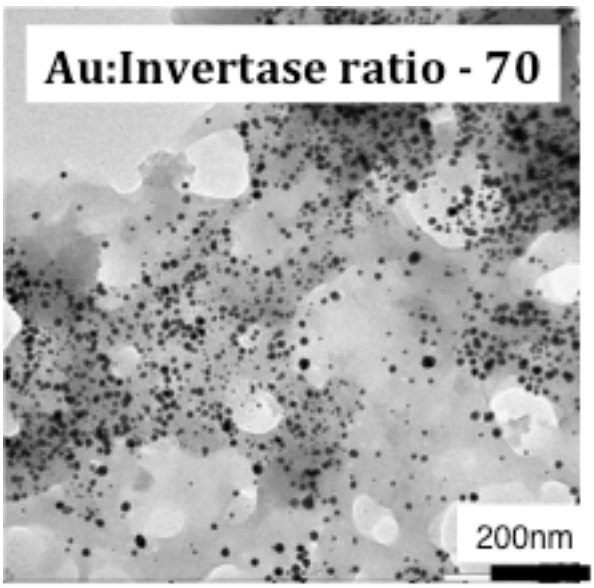

S10. TEM image of Myoglobin-AuNP fibers at a Au:Myoglobin ratio of 45

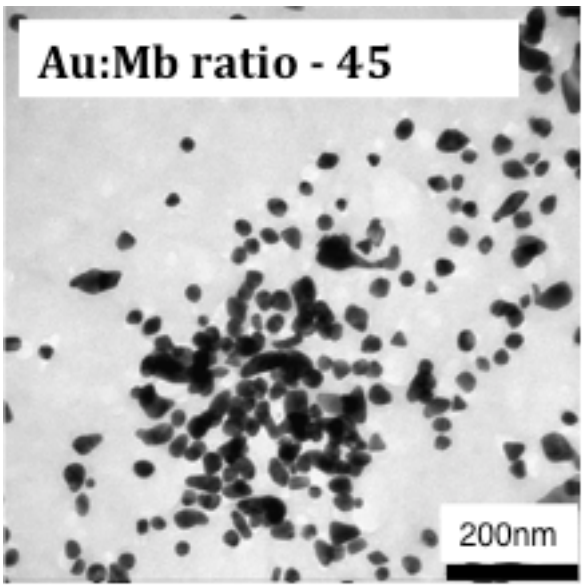

III. UV-Vis and AA data.

There are four distinct types of Au populations that are described in the UV-Vis. 1) No observed biotemplating reaction. 2) AuNP formation. 3) Precipitated protein-Au clusters. 4) AuNP-fiber formation. Several aspects of these graphs should be noted. 1) The individual proteins do not display each population described. 2) Population #4 only occurs at very low protein concentrations. 3) Some of the traces for fiber formation show some absorbance at 530 due to some of the fibers floating in solution after the centrifugation step.

S11. UV-Vis spectra of BSA biotemplating reactions

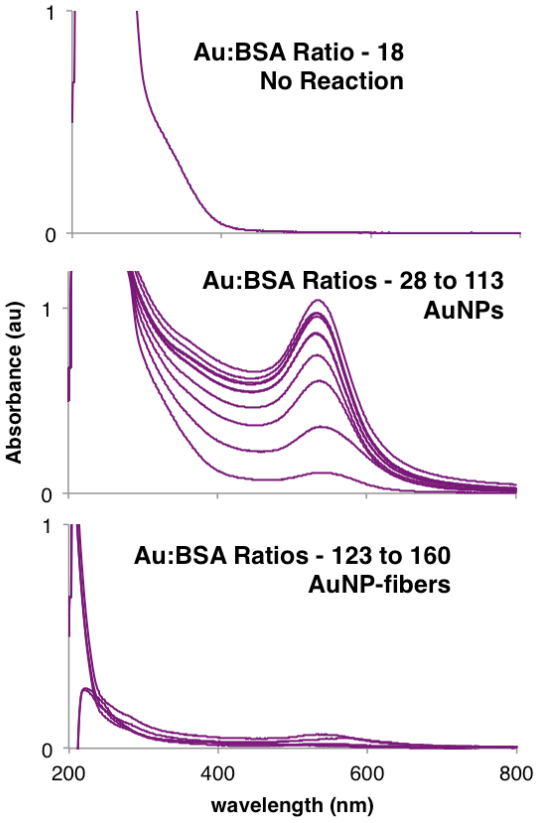

S12. UV-Vis spectra of catalase biotemplating reactions

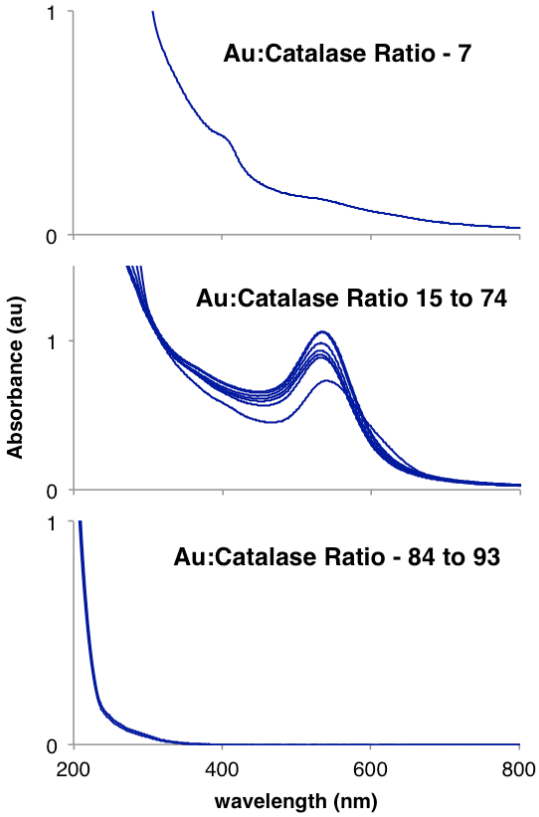

S13. UV-Vis spectra of hemoglobin biotemplating reactions

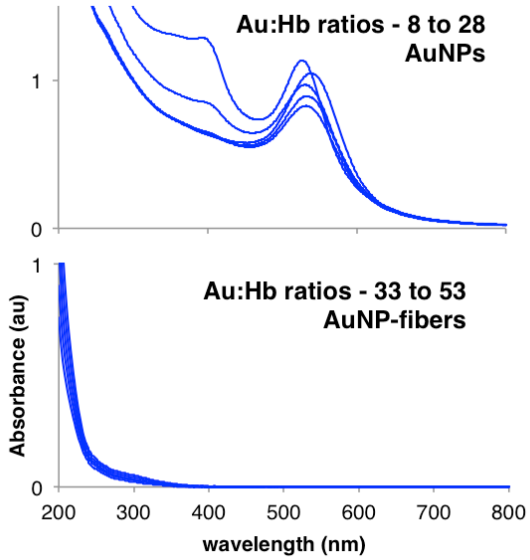

S14. UV-Vis spectra of lysozyme biotemplating reactions

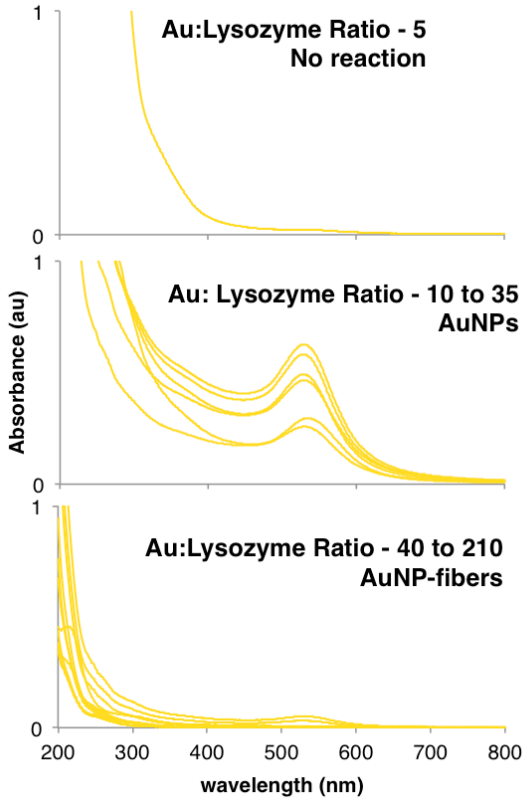

S15. UV-Vis spectra of myoglobin biotemplating reactions

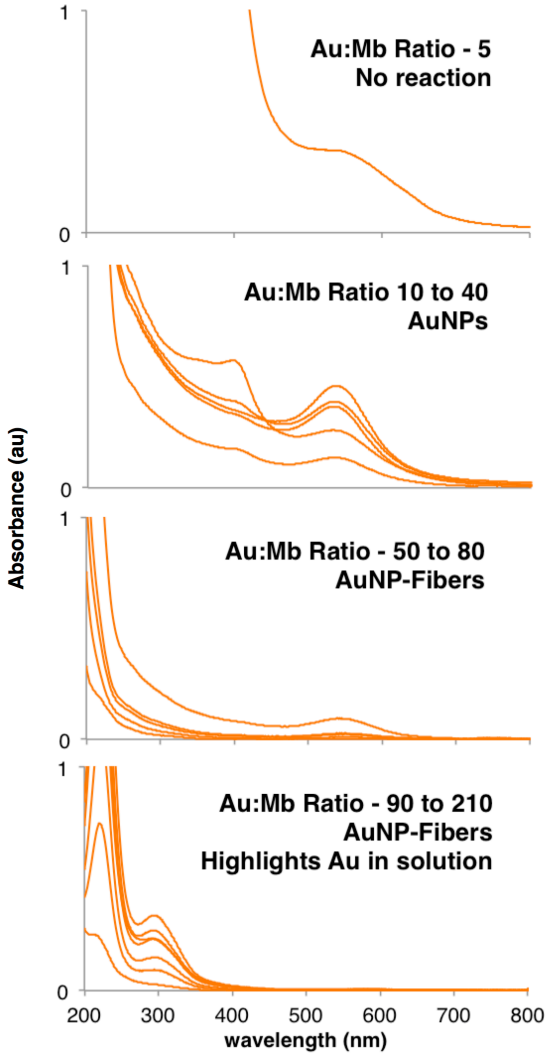

S16. UV-Vis spectra of pepsin biotemplating reactions

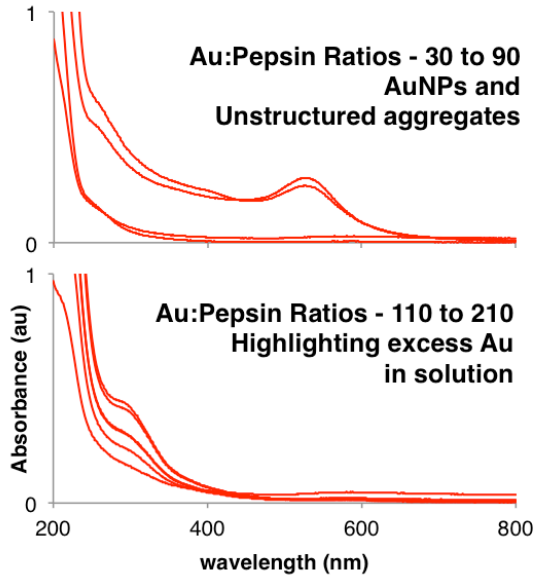

By plotting the absorbance value of the SPR feature (squares) along with the gold concentration as measured by AA (circles), we can determine the critical ratio, which describes the protein concentration where the biotemplating products change from AuNPs to AuNP fibers

S17. BSA-AuNP UV-Vis and AA data

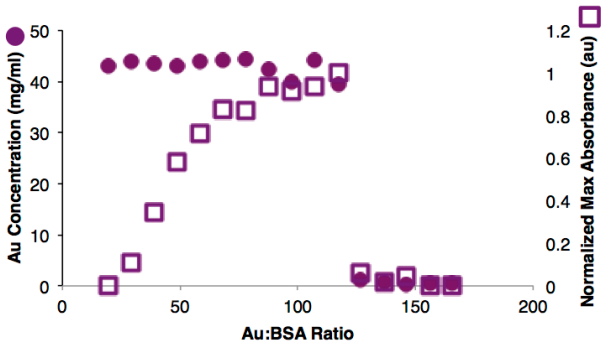

S18. Hemoglobin-AuNP UV-Vis and AA-data

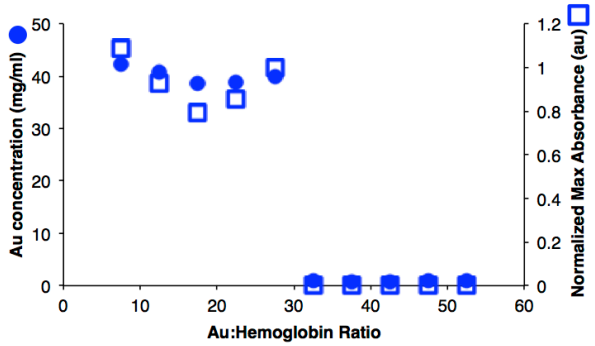

S19. Lysozyme-AuNP UV-Vis and AA-data

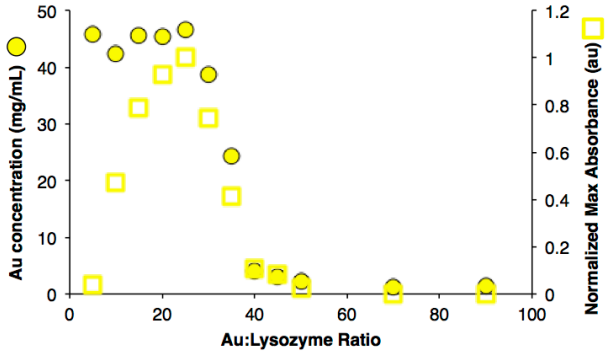

S20. Myoglobin-AuNP UV-Vis and AA-data

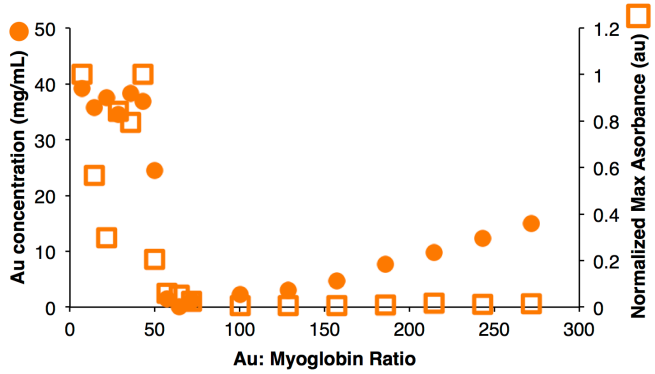

S21. Pepsin-AuNP UV-Vis and AA-data

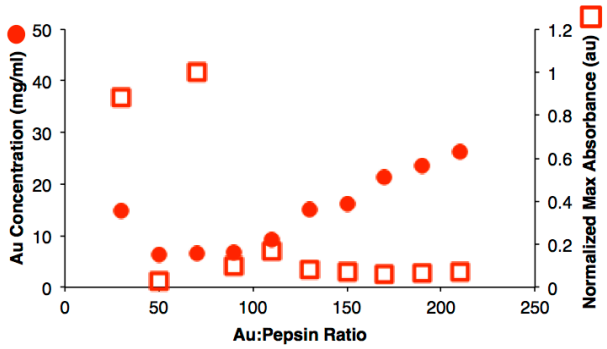

IV. Gold nanoparticle formation kinetics

Nanoparticle formation kinetics were analyzed from spectra recorded with an Ocean Optics Jaz spectrometer. A capped cuvette, containing the reaction mixture, was placed in a temperature controlled cuvette holder (qpod 2e from Quantum Northwest). Individual spectra were recorded every 120 seconds (in most cases) until the nanoparticle formation reaction had nearly reached its end point. Reactions were monitored at 60, 70, 80, and 90 °C. The kinetics of nanoparticle formation was analyzed by subtracting the absorption minimum (just before the localized surface plasmon feature, LSP) from the absorption at the LSP maximum. These features are indicated in Figure S27. These ΔA values are then normalized to better highlight the reaction endpoints.

S27. Spectra from multiple times for the reaction of BSA with $HAuCl_4$. Figure highlights the data analysis used for evaluating the reaction kinetics.

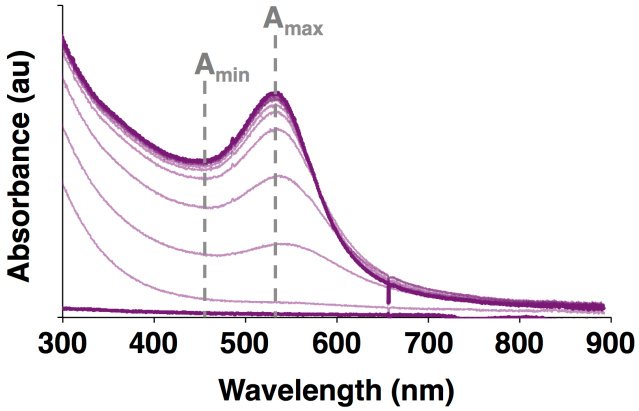

S28. Normalized(A_{max}-A_{min}) vs. time for BSA at 60, 70, 80, and 90 °C for Au:BSA ratios of 90 (purple), which produce homogenous BSA-AuNPs, and 150 (gray), which produce BSA-AuNP fibers.

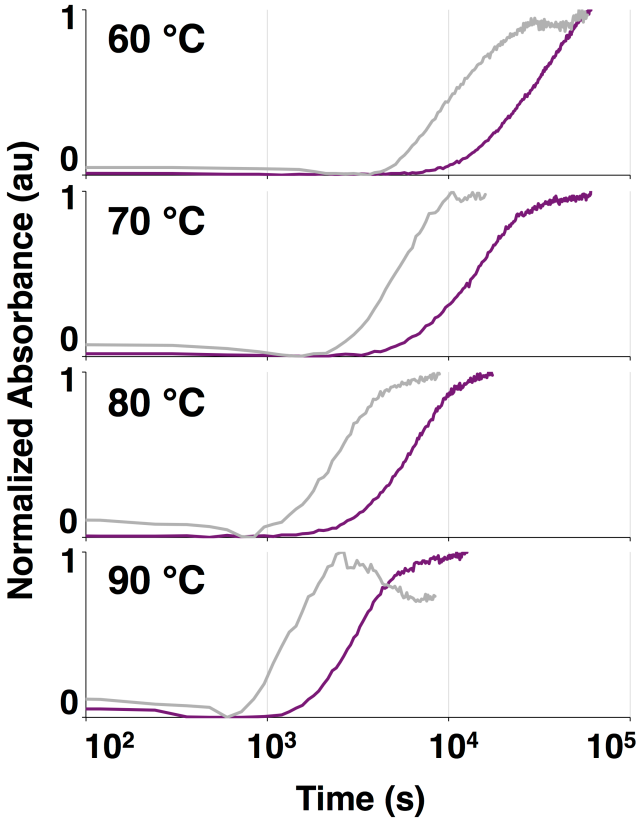

S29. Normalized(A_{max}-A_{min}) vs. time for catalase at 60, 70, 80, and 90 °C for Au:catalase ratios of 60 (dark blue), which produce homogenous catalase-AuNPs, and 110 (gray), which produce catalase-AuNP fibers.

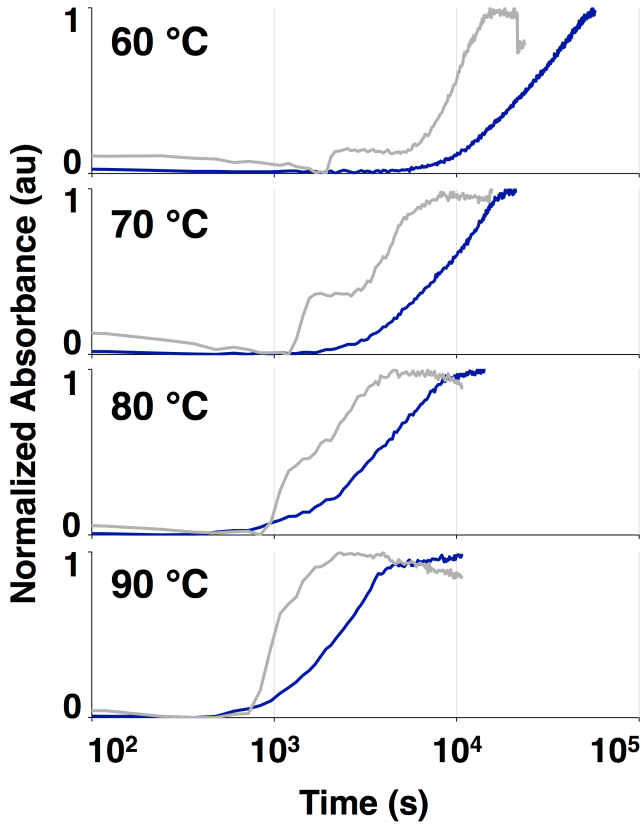

S30. Normalized(A_{max}-A_{min}) vs. time for hemoglobin at 60, 70, 80, and 90 °C for Au:hemoglobin ratios of 20 (blue), which produce homogenous hemoglobin-AuNPs, and 40 (gray), which produce hemoglobin-AuNP fibers.

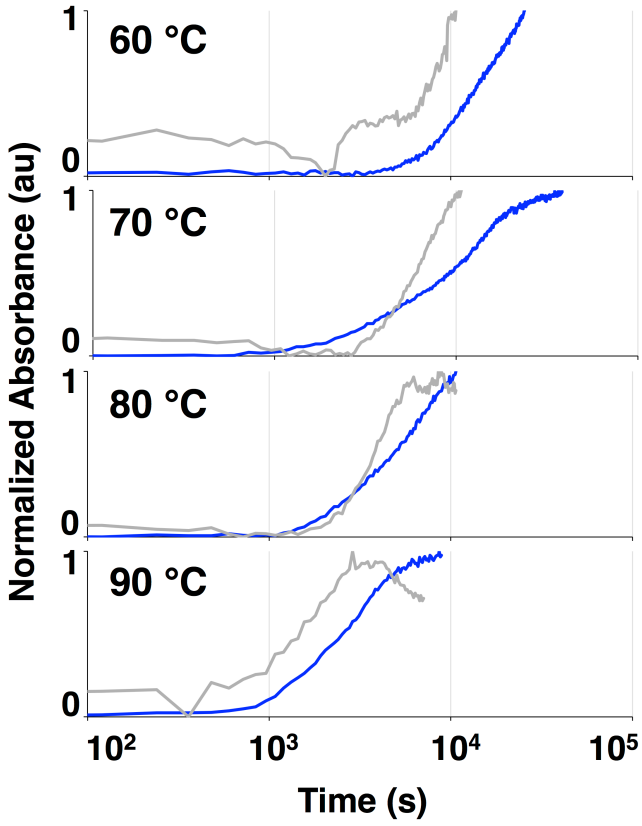

S31. Normalized(A_{max}-A_{min}) vs. time for lysozyme at 60, 70, 80, and 90 °C for Au:lysozyme ratios of 25 (blue), which produce homogenous lysozyme-AuNPs, and 55 (gray), which produce lysozyme-AuNP fibers.

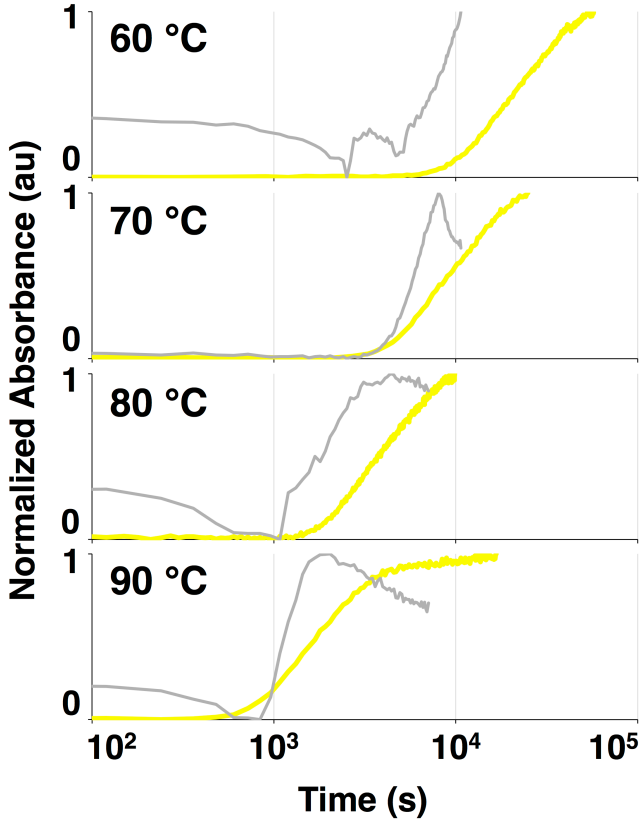

Table 1. Proteins, AuNP/AuNP fiber critical ratio values, and biotemplating relevant protein properties.

	BSA	Catalase	Hemoglobin	HRP	Invertase	Lysozyme	Myoglobin	Pepsin
Critical Ratio (moles Au:moles protein)	**125**	**80**	**30**	-	-	**35**	**35**	-
Critical Ratio (moles Au:10^3 g protein)	1.9	1.3	1.9	-	-	2.4	2.1	-
Molecular Weight (Da)	66,430	62,500	16,125	44,000	270,000	14,307	17,600	34,620
Number of Ligating Amino Acids[a]	153	103	24	43	77	20	35	52
Number of Reducing Amino Acids[a]	36	26	4	10	49	11	5	24
pI	5.3[2]	5.4[3]	6.8[4]	3-9[5]	4[6]	11.35[7]	7.3[8]	2.5[9]
% Structured[a]	76	56	82	47	52	74	57	71
Secondary Structure Unfolding Temperature (°C)	80[10]	56[11]	65[12]	82[13]	-	70[14]	80[15]	63[16]
Tertiary Structure Unfolding Temperature (°C)	68[17]	56[11]	50[18]	55[13]	65[19]	65[20]	75[21]	63[22]
Average Protein Hopp-Woods Hydrophobicity[b]	0.281	0.048	-0.081	-0.100	-0.154	-0.048	0.170	-0.282

[a]The numbers of ligating and reducing amino acids and the percentage of the protein that is structured were taken from data in UniProt.[23] (BSA - UniProt code: P02769, catalase - P00432, hemoglobin - P07020 and P01966, invertase - P10594, lysozyme - P00698, myoglobin - P68082, and pepsin - P00791). Structural data from HRP was gathered from a specific crystal structure.[24]

[b]The average Hopp-Woods[25] hydrophobicity measurement was performed using the ExPasy tools.[26]

V. References

1. M. R. Hartings, N. Benjamin, F. Briere, M. Briscione, O. Choudary, T. L. Fisher, L. Flynn, E. Ghias, M. Harper, N. Khamis, C. Koenigsknecht, K. Lazor, S. Moss, E. Robbins, S. Schultz, S. Yaman, L. M. Haverhals, P. C. Trulove, H. C. De Long, A. E. Miller and D. M. Fox, *Sci. Technol. Adv. Mat.*, 2013, **14**.
2. J. F. Foster and L. J. Kaplan, *Biochemistry*, 1971, **10**, 630-636.
3. T. Samejima, M. Kamata and K. Shibata, *J. Biochem.*, 1962, **51**, 181-187.
4. H. Kon and M. W. Makinen, *Biochemistry*, 1971, **10**, 43-52.
5. L. M. Shannon, E. Kay and J. Y. Lew, *J. Biol. Chem.*, 1966, **241**, 2166-2172.
6. P. G. Righetti and T. Caravaggio, *J. Chromatog. A*, 1976, **127**, 1-28.
7. L. R. Wetter and H. F. Deutsch, *J. Biol. Chem.*, 1951, **192**, 237-242.
8. B. J. Radola, *BBA-Prot. Struct.*, 1973, **295**, 412-428.
9. D. Malamud and J. W. Drysdale, *Anal. Biochem.*, 1978, **86**, 620-647.
10. Y. Moriyama, E. Watanabe, K. Kobayashi, H. Harano, E. Inui and K. Takeda, *J. Phys. Chem. B*, 2008, **112**, 16585-16589.
11. J. Switala, J. O. O'Neil and P. C. Loewen, *Biochemistry*, 1999, **38**, 3895-3901.
12. A. Michnik, Z. Drzazga, A. Kluczewska and K. Michalik, *Biophys. Chem.*, 2005, **118**, 93-101.
13. K. Chattopadhyay and S. Mazumdar, *Biochemistry*, 1999, **39**, 263-270.
14. Y. J. Shiu, U. S. Jeng, Y. S. Huang, Y. H. Lai, H. F. Lu, C. T. Liang, I. J. Hso, C. H. Su, C. Su, I. Chao, A. C. Su and S. H. Lin, *Biophys. J.*, 2008, **94**, 4828-4836.
15. Y. Moriyama and K. Takeda, *J. Phys. Chem. B*, 2010, **114**, 2430-2434.
16. S. R. Tello-Solis and B. Romero-Garcia, *Int. J. Biol. Macromol.*, 2001, **28**, 129-133.
17. A. Michnik, K. Michalik, A. Kluczewska and Z. Drzazga, *J. Therm. Anal. Calorim.*, 2006, **84**, 113-117.
18. Y. B. Yan, Q. Wang, H. W. He and H. M. Zhou, *Biophys. J.*, 2004, **86**, 1682-1690.
19. D. Cavaille and D. Combes, *J. Biotechnol.*, 1995, **43**, 221-228.
20. F. Meersman, C. Atilgan, A. J. Miles, R. Bader, W. F. Shang, A. Matagne, B. A. Wallace and M. H. J. Koch, *Biophys. J.*, 2010, **99**, 2255-2263.
21. F. Meersman, L. Smeller and K. Heremans, *Biophys. J.*, 2002, **82**, 2635-2644.
22. V. M. Pavelkic, M. V. Beljanski, K. M. Antic, M. M. Babic, T. P. Brdaric and K. R. Gopcevic, *Russ. J. Phys. Chem. A*, 2011, **85**, 2245-2250.
23. M. Magrane and C. UniProt, *Database*, 2011.
24. G. I. Berglund, G. H. Carlsson, A. T. Smith, H. Szoke, A. Henriksen and J. Hajdu, *Nature*, 2002, **417**, 463-468.
25. T. P. Hopp and K. R. Woods, *Proc. Natl. Acad. Sci., USA*, 1981, **78**, 3824-3828.
26. E. Gasteiger, A. Gattiker, C. Hoogland, I. Ivanyi, R. D. Appel and A. Bairoch, *Nucleic Acids Res.*, 2003, **31**, 3784-3788.